NEOPLASIA
www.neoplasia.com

Volume 13 Number 3 March 2011 pp. 276–285 276

Imaging Bone Morphogenetic Protein 7 Induced Cell Cycle Arrest in Experimental Gliomas[1,2]

Anke Klose*, Yannic Waerzeggers*, Parisa Monfared*, Slobodan Vukicevic†, Eric L. Kaijzel‡, Alexandra Winkeler*, Claudia Wickenhauser‡, Clemens W. G. M. Löwik§ and Andreas H. Jacobs*

*European Institute for Molecular Imaging, University of Münster, Germany and MPI for Neurological Research, Cologne, Germany; †Department of Anatomy, School of Medicine, Zagreb, Croatia; ‡Department of Pathology, Faculty of Medicine of the University of Leipzig, Leipzig, Germany; §Department of Endocrinology and Metabolic Diseases, Leiden University Medical Center, Leiden, The Netherlands

Abstract

Bone morphogenetic protein 7 (BMP-7) belongs to the superfamily of transforming growth factor β–like cytokines, which can act either as tumor suppressors or as tumor promoters depending on cell type and differentiation. Our investigations focused on analyzing the effects of BMP-7 during glioma cell proliferation *in vitro* and *in vivo*. BMP-7 treatment decreased the proliferation of Gli36ΔEGFR-LITG glioma cells up to 50% through a cell cycle arrest in the G_1 phase but not by induction of apoptosis. This effect was mediated by the modulation of the expression and phosphorylation of cyclin-dependent kinase 2, cyclin-dependent kinase inhibitor p21, and downstream retinoblastoma protein. Furthermore, *in vivo* optical imaging of luciferase activity of Gli36ΔEGFR-LITG cells implanted intracranially into nude mice in the presence or absence of BMP-7 treatment corroborated the antiproliferative effects of this cytokine. This report clearly underlines the tumor-suppressive role of BMP-7 in glioma-derived cells. Taken together, our results indicate that manipulating the BMP/transforming growth factor β signaling cascade may serve as a new strategy for imaging-guided molecular-targeted therapy of malignant gliomas.

Neoplasia (2011) 13, 276–285

Introduction

Glioblastoma multiforme (GBM) is the most aggressive primary glial tumor of the brain, with an average life expectancy of 1 year or less [1]. Therefore, therapeutic approaches are needed to treat tumors more effectively by targeting molecular signal transduction pathways involved in cancer progression directly. Deregulation of growth factor or growth factor receptor expression is one of the characteristic features of GBM. One pathway frequently affected during gliomagenesis is the transforming growth factor β (TGF-β) signaling pathway [2,3]. This pathway is often referred to as a double-edged sword because the tumor-suppressive activity of TGF-β can switch to be a stimulator of malignant progression [4–6].

Bone morphogenetic proteins (BMPs) are cytokines belonging to the TGF-β superfamily, whose members reveal a variety of biologic functions such as proliferation and apoptosis [7,8]. The biologic effects of BMPs as well as of TGF-β are mediated by cytosolic Smad-dependent and several Smad-independent intracellular signaling pathways [5]. To signal through the canonical BMP pathway, dimeric cytokines bind to heterotetrameric receptor complexes on the cell surface composed of type I and II receptor homodimers. Activated type I receptors initiate

Abbreviations: BMP, bone morphogenetic protein; Cdk, cyclin-dependent kinase; CdkI, cyclin-dependent kinase inhibitor; LITG, *firefly luciferase*-IRES-*tkgfp*; Rb, retinoblastoma protein

Address all correspondence to: Univ.-Prof. Dr. Andreas H. Jacobs, European Institute for Molecular Imaging, University of Münster, Germany. E-mail: ahjacobs@uni-muenster.de

[1]This work was supported in part by the Center for Molecular Medicine Cologne (CMMC-TV46), 6th FW EU grant EMIL (LSHC-CT-2004-503569), DiMI (LSHB-CT-2005-512146), and CLINIGENE (LSHB-CT-2006).

[2]This article refers to supplementary materials, which are designated Table W1 and Figures W1 to W4 and are available online at www.neoplasia.com.

Received 9 November 2010; Revised 21 December 2010; Accepted 30 December 2010

DOI 10.1593/neo.101540

downstream signaling by phosphorylation of receptor-regulated Smad proteins (R-Smads), which form complexes with Smad-4 (Co-Smad) to translocate into the nucleus and initiate target gene transcription. Heteromeric combination of TGF-β superfamily receptors, R-Smad–Co-Smad complex formation, and regulation by inhibitory Smads point out at the complexity of the TGF-β superfamily signaling [9,10].

TGF-β, BMPs as well as the other members of this superfamily, is a potent inhibitor of growth, such as epithelial and endothelial cell growth, but reveals mitogenic properties in mesenchymal-derived cells. Two events are known to mediate the TGF-β–induced growth arrest in mid- and late-G_1 phases of the cell cycle: inactivation of cyclin-dependent kinases (Cdks) and down-regulation of c-*myc* [11,12]. The transition from G_1 to S phase in the mammalian cell cycle is cooperatively regulated by cyclins, Cdks, and Cdk inhibitors (CdkIs). The first class of CdkIs that specifically inhibit Cdk4 and Cdk6 includes the INK4A proteins ($p16^{INK4A}$, $p15^{INK4B}$, $p18^{INK4C}$, and $p19^{INK4D}$), whereas members of the Cip/Kip family of inhibitors ($p21^{Cip1/Waf1}$, $p27^{Kip1}$, and $p57^{Kip2}$) reveal a broader inhibition spectrum. Progression in the cell cycle involves phosphorylation of the retinoblastoma protein (Rb) tumor-suppressor gene product pRb [13]. Similar to TGF-β, BMPs have also been shown to influence cell proliferation and apoptosis. Suppression of tumor formation in skin by induction of apoptosis was reported on the overexpression of BMP-6 [14]; similarly, the anti-tumor effect of BMP-5, -6, and -7 in human myeloma cells was also mediated by the induced apoptosis [15]. BMP signaling has been demonstrated to be growth suppressive in colon cancer cells [16]. Cell cycle arrest, induced by upregulation of $p21^{Cip1}$ and $p27^{Kip1}$, was reported for BMP-7–treated thyroid carcinoma cells [17]. Growth inhibition of BMP-2–treated breast carcinoma cells revealed to be a consequence of $p21^{Cip1/Waf1}$ upregulation, inhibition of Cdk2, and hypophosphorylation of pRb [18]. The same results were obtained by Miyazaki et al. [19] after administration of BMP-7 *in vitro* and overexpression of constitutively active Alk-6 receptor in androgen-insensitive prostate cancer cells *in vivo*. BMP-7 also counteracted breast cancer growth at the primary site and in bone metastasis *in vivo* [20]. Already in 1996, Yamada et al. [21] demonstrated the progressive expression of Alk-6 in malignant glioma tumors. More recently, it has been shown that BMPs promote differentiation, thereby depleting the pool of brain tumor–initiating cells [22,23].

In the following study, we focused on elucidating how BMP-7 influences glioma cell growth *in vitro* and analyzed the underlying molecular mechanisms. In addition, by optical imaging, we could monitor and confirm *in vivo* antiproliferative effects of BMP-7 in experimental gliomas. Our results presented herein provide evidence for the striking role of BMP-7 in regulatory processes of glioma cell proliferation.

Materials and Methods

Antibodies, Material, and Enzymes

The monoclonal mouse antibody directed against human $p21^{Cip1/Waf1}$ (DCS60) as well as the polyclonal rabbit antibodies anti-human $p15^{INK4B}$, $p16^{INK4A}$, $p27^{Kip1}$, phospho-Rb (Ser795), phospho-Rb (Ser807/811), and phospho-Cdk2 (Thr160) and the horseradish peroxidase–labeled secondary antibodies, goat anti–mouse immunoglobulin G, and goat anti-rabbit immunoglobulin G were obtained from Cell Signaling Technology, Inc (Danvers, MA) and used according to the manufacturer's instructions. Monoclonal mouse anti–human actin (C4) was purchased from ImmunO (dilution 1:10000; MP Biomedicals, Inc, Aurora, OH). Polyclonal rabbit anti–human phospho-SMAD-1(Ser463/465)/-5(Ser463/465)/-8(Ser426/428) was from Chemicon International (Hampshire, UK; dilution 1:1000 for Western blot and 1:100 for immunofluorescence analysis). For immunofluorescence analysis, goat anti–rabbit Cy3 (FluorolinkCy3, CyDye; Amersham Pharmacia Biotech, Uppsala, Sweden; dilution 1:500) served as a secondary antibody. D-Luciferin potassium salt was purchased from Synchem OHG (Felsberg/Altenburg, Germany). Human recombinant BMP-7 was dissolved in 20-mM sodium acetate trihydrate buffer with 5% (wt/vol) mannitol (pH 4.5), which also served as control buffer throughout all experiments.

Cell Culture

The seven human glioblastoma–derived cell lines used were Gli36-ΔEGFR, Gli36wt, and U87 MG (kind gifts of Dr David Louis, Molecular Neurooncology Laboratory, MGH, Boston, MA); U87ΔEGFR (kind gift of Dr H.-J. Su Huang, Ludwig Institute for Cancer Research, San Diego, CA); A172 and G55T2 (both kind gifts of Prof. U. Schlegel, Department of Neurology, University Hospital Bonn, Bonn, Germany); and U251 (kind gift of Prof. J. Hampl, Department of Neurosurgery, University of Cologne, Cologne, Germany). All cells were cultured in Dulbecco modified Eagle medium high glucose (4.5 g/L) with L-glutamine and sodium pyruvate (PAA Laboratories GmbH, Pasching, Austria) enriched with 10% (vol/vol) fetal calf serum (FCS; PAA Laboratories GmbH), 100 U/ml penicillin and 100 μg/ml streptomycin (P/S; PAA Laboratories GmbH) at 37°C in a 5% CO_2/95% air atmosphere. Gli36ΔEGFR and U87ΔEGFR cells were cultured in the additional presence of the following selection antibiotics, 2 μg/ml puromycin (Sigma-Aldrich Chemie GmbH, München, Germany) and 500 μg/ml G418 (Invitrogen Life Technologies, Karlsruhe, Germany), respectively. All cell lines were cultured as monolayers and routinely passaged by trypsinization. The retrovirally transduced cell lines Gli36ΔEGFR-LITG and U87ΔEGFR-LITG were cultured under the same conditions.

Generation of Gli36ΔEGFR-LITG and U87ΔEGFR-LITG Stable Cell Lines

The generation of the pBABE-LITG plasmid was based on the construct pBABE-CITG (cytosine deaminase-IRES-*tkgfp*), which was generated by transferring the expression cassette CITG from pHSV-CITG [24] into pBABE-puromycin. The luciferase gene, together with the Kozak sequence, was amplified by polymerase chain reaction (PCR) using the pTA-luc plasmid (Clontech-Takara Bio Europe, Saint-Germain-en-Laye, France) as a template. The PCR amplicon, flanked by 5′ *Xho*I and 3′ *Bgl*II restriction sites, was ligated into the pBABE-ITG (IRES-*tkgfp*) backbone originated after *Xho*I/*Bgl*II digestion of pBABE-CITG. Retroviral packaging was described previously [24].

RNA Isolation and Reverse Transcription–PCR

Total RNA was isolated from human glioblastoma–derived cell lines using RNeasy Plus Mini Kit and RNeasy Fibrous Tissue Mini Kit according to the manufacturer's instructions (Qiagen, Hilden, Germany). Two micrograms of total RNA was reverse-transcribed according to the manufacturer's instructions (SuperScript II RNAse H^- Reverse Transcriptase; Invitrogen GmbH) using oligo d/T (Invitrogen GmbH) as primers. PCR amplification was performed using the HotStarTaq Master Mix Kit (Qiagen) with specific primers for TGF-β superfamily signaling molecules (Table W1). Amplification of β-actin complementary DNA was used as a positive control of each PCR. Negative controls

were performed for each primer pair by omitting the corresponding complementary DNA template. Numbers of cycles, specific annealing temperatures, and extension times are provided in Table W1. PCR products were separated by electrophoresis in agarose gel (1% (wt/vol)) and visualized with ethidium bromide. Amplified fragments were identified by size and by sequencing after purification with QIAquick PCR Purification Kit (Qiagen) according to the manufacturer's instructions. Primer pairs were generated by using PerlPrimer v1.1.10 Software (free software http://perlprimer.sourceforge.net). The origin of primer pairs, which were not generated with this software, is given in Table W1.

Immunofluorescence

Immunofluorescence analysis was performed using standard procedures. Cells were seeded at a density of 1.5×10^5/well in a 24-well plate and incubated for 24 hours in corresponding medium containing only 1% (vol/vol) FCS. After treatment with human recombinant BMP-7 (500 ng/ml) or control buffer for 30, 60, and 90 minutes, cells were fixed with 4% (vol/vol) paraformaldehyde/phosphate-buffered saline (PBS) and permeabilized with 0.5% (vol/vol) Triton/PBS. Blocking of unspecific binding sites was performed with 10% (wt/vol) BSA/PBS containing 0.05% (vol/vol) Triton followed by incubation with primary (rabbit anti–human phospho-SMAD-1/-5/-8) and secondary antibodies (goat anti–rabbit Cy3). Cells were mounted with AquaPoly/Mount (Polysciences, Inc, Warrington, PA), and fluorescence was monitored with a Zeiss Axiovert 135 fluorescence microscope (Carl Zeiss, Heidenheim, Germany). Photographs were prepared using an INTAS digital camera (Göttingen, Germany).

Cell Cycle Analysis

Cells were seeded at a density of 3.6×10^5 cells/6-cm dish and incubated for 24 hours in medium containing only 1% (vol/vol) FCS. After 24 hours of stimulation with human recombinant BMP-7 (500 ng/ml) or control buffer, all cells were collected, washed twice in PBS, and frozen in EtOH. Cellular DNA was stained with propidium iodide (Sigma-Aldrich Chemie GmbH) according to the methods described by Vindelov et al. [25–28]. The cellular DNA content was analyzed by flow cytometry (FACSCalibur; Becton Dickinson, Heidelberg, Germany). All experiments were done in triplicate.

Cell Proliferation

To analyze the effects of BMP-7 on Gli36ΔEGFR-LITG cell proliferation, cells were seeded at a density of 3×10^4 cells/well in a 24-well plate and incubated in medium containing 1% (vol/vol) FCS. After 24 hours, control cells were harvested and counted before starting the cytokine treatment (0 hour). Cells were stimulated with BMP-7 (500 ng/ml) or control buffer for 24, 48, 72, and 96 hours. Fresh cytokine or control buffer was added to corresponding wells 48 hours after initial stimulation because recombinant BMP-7 was not stable over the time in cell culture medium. After stimulation, cells were trypsinized and counted using cell Fast-Read 102 counting chambers (Biosigma s.r.l., Cona, Italy), and dead cells were visualized by Trypan blue staining (0.2% [vol/vol]; bioWhittaker, Inc, Walkersville, MD). All experiments were performed six times.

In addition, cell proliferation was monitored by bioluminescence imaging of luciferase activity using an IVIS200 optical imaging system (Xenogen Corp). Gli36ΔEGFR-LITG cells were seeded and cultured as described above followed by treatment with BMP-7 (500 ng/ml) or control buffer for 48 hours. Bioluminescence was detected 8 minutes after adding D-luciferin (80 μg/well in 40 μl of PBS). Images were acquired at standard camera settings for bioluminescence imaging with exposure times of 5 seconds to 1 minute. Data evaluation based on ROI (region of interest) analysis of bioluminescence images was performed by the use of Living Image Software version 2.50 (Xenogen Corp) to determine total flux values (photons/sec). All experiments were done in triplicate.

Caspase-3/-7 Activity Assay

Caspase-3/-7 activity was determined using the Caspase-Glo 3/7 Assay (Promega, Mannheim, Germany) according to the manufacturer's instructions. Gli36ΔEGFR-LITG cells were seeded at a density of 5×10^3 cells/well in a 96-well and incubated in medium containing 1% (vol/vol) FCS for 24 hours. Cells were treated with BMP-7 (500 ng/ml) or control buffer for 24, 48, and 96 hours. Fresh cytokine or control buffer was added to corresponding wells 48 hours after initial stimulation. After treatment, 100 μl of Caspase-Glo Reagent was added to each well and incubated for 1 hour at 37°C. Luminescence was monitored using a Mithras LB 940 plate reader (Berthold Technologies, Bad Wildbad, Germany). All experiments were performed in triplicate.

Preparation of Cell Lysates and Immunoblot Analysis

Cells were seeded at a density of 1.5×10^6 cells/6-cm-diameter dish in medium containing 1% (vol/vol) FCS and cultured in the absence/presence of human recombinant BMP-7 (500 ng/ml) for 1, 6, 24, and 48 hours. Cells were collected by scraping, and lysates were prepared as described previously [29] in the presence of 1 mM sodium orthovanadate (Sigma-Aldrich Chemie GmbH). Cell lysates, 50 μg, were resolved by SDS-PAGE using Novex 14% (wt/vol) Tris-glycine gels (Invitrogen GmbH). Proteins were transferred to Hybond-C Extra (Amersham Biosciences, Braunschweig, Germany). Immunoblot analysis was performed as described previously [29] in the presence of 50 mM NaF. All experiments were quantified by determining the signal intensities using ImageJ 1.32j software (Wayne Rasband, National Institutes of Health) and normalized to the signal intensities of the β-actin loading control.

Animals

All animal experiments were in accordance with the National Institutes of Health guidelines and approved by the local animal care committee (Bezirksregierung Köln).

Gli36ΔEGFR-LITG cells (1×10^5) were implanted intracranially into the striatum of immune-deficient mice (BALB/cA nude). For intravenous administration of recombinant BMP-7, microports (Style I Catheter Microport for vascular access in mice; Braintree Scientific, Inc, Braintree, MA) were implanted into the v. jugularis. Cell proliferation *in vivo* was monitored by bioluminescence imaging. After tumor establishment (day 0) indicated by a total flux of 150,000 photons/sec, mice were treated daily with the cytokine (100 μg/kg per day).

Bioluminescence Imaging of Luciferase Activity In Vivo

Analysis of luciferase gene expression was performed on an IVIS200 optical imaging system (Xenogen Corp). Bioluminescence imaging was performed to monitor tumor growth. When tumors were established, imaging was performed at day 0 (before treatment) to measure the total flux of established tumors and to calculate the *x*-fold induction of total flux at several time points after starting the therapy for each animal individually. For bioluminescence detection, mice were injected intraperitoneally with D-luciferin (4 mg/animal in 200 μl of PBS), and

images were acquired 8 minutes after luciferin injection at standard camera settings for bioluminescence imaging with exposure times of 10 seconds to 1 minute. Data evaluation based on ROI analysis of bioluminescence images was performed by the use of Living Image Software version 2.50 (Xenogen Corp) to determine total flux values (photons/sec). Data were background subtracted after analyzing total flux values of luciferase negative parts of mouse bodies with identical ROIs.

Statistics

Student's *t* test was performed with SigmaStat 3.0 (SPSS, Inc., Chicago, IL) or with Microsoft Office Excel (Unterschleißheim, Germany) using a 2-tailed and heteroskedastic analysis. Level of significance was set at $P < .05$.

Results

Expression of TGF-β Superfamily Signaling Molecules in Different Human Glioblastoma–Derived Cell Lines

To characterize BMP-7 signaling in glioma *in vitro* and *in vivo*, we used a panel of well-characterized human glioblastoma–derived cell lines. In addition, two of the analyzed cell lines were retrovirally transduced, and cell lines stably expressing the imaging gene cassette coding for LITG (Gli36ΔEGFR-LITG and U87ΔEGFR-LITG) were generated. Analysis of transcripts expression for BMP-7, TGF-$\beta_{1\text{-}3}$, their relevant type I (Alk-1, -2, -3, -5, -6) and type II receptors (BMPRII, ActrIIA, ActrIIB, TβR-II) as well as downstream signaling Smad proteins (Smad-1, -2, -3, -4, -5, -6, -7, -8) was performed by RT-PCR (Figure 1).

All cell lines expressed TGF-β_1, Alk-2 and -5, BMPRII, ActrIIA, ActrIIB, Smad-1, -3, -4, -5, and -8 messenger RNA (mRNA). TGF-β_3 transcripts were not detected exclusively in A172 cells. Alk-1 mRNA could only be observed in A172 cells, whereas Alk-5 transcripts were absent in U251 and A172 cells. Gli36ΔEGFR-LITG cells expressed nearly no TGF-β_2 and only low levels of Alk-5 mRNA. Alk-6 transcripts were nearly missing in Gli36ΔEGFR-LITG and absent in A172 cells.

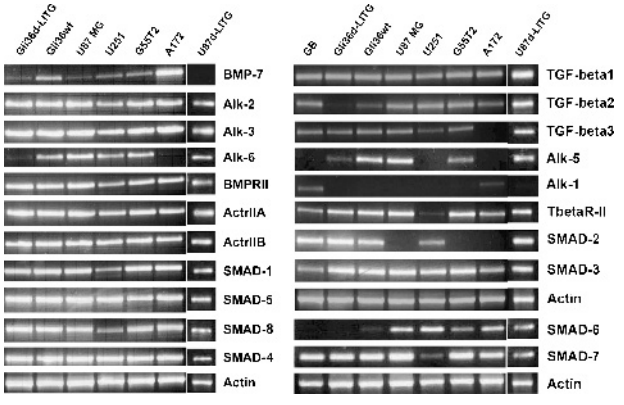

Figure 1. mRNA expression profile of TGF-β superfamily signaling molecules in various human glioblastoma–derived cell lines. Total cellular RNA was subjected to RT-PCR analysis with specific primer pairs, and amplicons were visualized by recording ethidium bromide fluorescence. Names of analyzed cell lines are presented above corresponding lanes (*d* = ΔEGFR).

U251 cells showed just weak amounts of TβR-II and Smad-7 mRNA. Smad-6 transcripts were not detectable in Gli36ΔEGFR-LITG cells, whereas Gli36wt cells expressed low amounts of these transcripts. U87 MG, G55T2, and A172 all lacked Smad-2 mRNA. Three cell lines represented variable expression profiles of molecules of the intracellular BMP-7 signaling. Gli36ΔEGFR-LITG cells expressed only low levels of BMP-7 and Alk-6 and no Smad-6 mRNA, whereas A172 cells expressed high levels of BMP-7 and Smad-6 mRNA but lacked Alk-6, and U87ΔEGFR-LITG cells did not express BMP-7 but expressed Alk-6 and Smad-6 transcripts. Because of the different gene profiles, we chose Gli36ΔEGFR-LITG, A172, and U87ΔEGFR-LITG cells to further analyze BMP-7 signaling *in vitro*.

BMP-7 Downstream Signaling in Human Glioblastoma–Derived Cell Lines

Before studying BMP-7 signaling effects in cell culture, we analyzed if and how BMP-7 signals were transduced across the plasma membrane of Gli36ΔEGFR-LITG, A172, and U87ΔEGFR-LITG cells. By immunofluorescence, we analyzed phosphorylated regulatory Smad-1/-5/-8 in cultured cells as well as by immunoblot analysis of cell lysates after cells were treated with recombinant BMP-7 or control buffer (Figure 2).

All three cell lines responded to BMP-7 treatment in cell culture. Immunofluorescence staining of phosphorylated Smad-1/-5/-8 revealed the highest levels of activated Smad proteins in A172 and Gli36ΔEGFR-LITG cells already 30 and 60 minutes after cytokine treatment, respectively (Figure 2*A*), whereas in U87ΔEGFR-LITG cells, the highest levels of phosphorylated Smad proteins were attained within 90 minutes of BMP-7 treatment (Figure 2*A*). The same results were obtained after analyzing cell lysates derived from BMP-7 or control buffer–treated cells. Impressive amounts of activated regulatory Smad proteins could only be detected in cells treated with BMP-7. U87ΔEGFR-LITG cells responded slower (Figure 2*B*) to the cytokine treatment when compared with the other cell lines (Figure 2, *A* and *B*). Comparable amounts of phosphorylated Smad proteins were observed 24 hours after BMP-7 treatment (Figure 2*B*).

BMP-7 Induces G_1 Cell Cycle Arrest in Gli36ΔEGFR-LITG Cells

TGF-β and also BMPs have already been implicated in the regulation of the cell cycle. Because all three analyzed cell lines responded to BMP-7 stimulation, we further analyzed whether BMP-7 influences the cell cycling of each of the tested cell lines. Therefore, we performed cell cycle analysis 24 hours after BMP-7 stimulation (Figure 3). Plots resulting from FACS analysis of Gli36ΔEGFR-LITG cells are presented exemplarily (Figure 3*A*). The differences obtained during cell cycle analysis of all three cell lines were plotted inFigure 3*B*. We can clearly demonstrate that BMP-7 treatment increased the number of Gli36ΔEGFR-LITG cells being in G_1 up to 15.6%, whereas cell numbers in S and G_2/M phases were significantly reduced of approximately 45% and 22.3%, respectively, when compared with control buffer–treated cells (Figure 3*B*). Statistically significant results were also obtained regarding cytokine-treated A172 cells, where increased cell numbers in G_1 and decreased cell numbers in S and G_2/M phases were observed, although the effect in these cells was weaker when compared with stimulated Gli36ΔEGFR-LITG cells (Figure 3*B*). However, U87ΔEGFR-LITG cells showed an opposite behavior after cytokine treatment. The number of cells being in G_1 phase was decreased, whereas the number of cells being in S and G_2/M phases

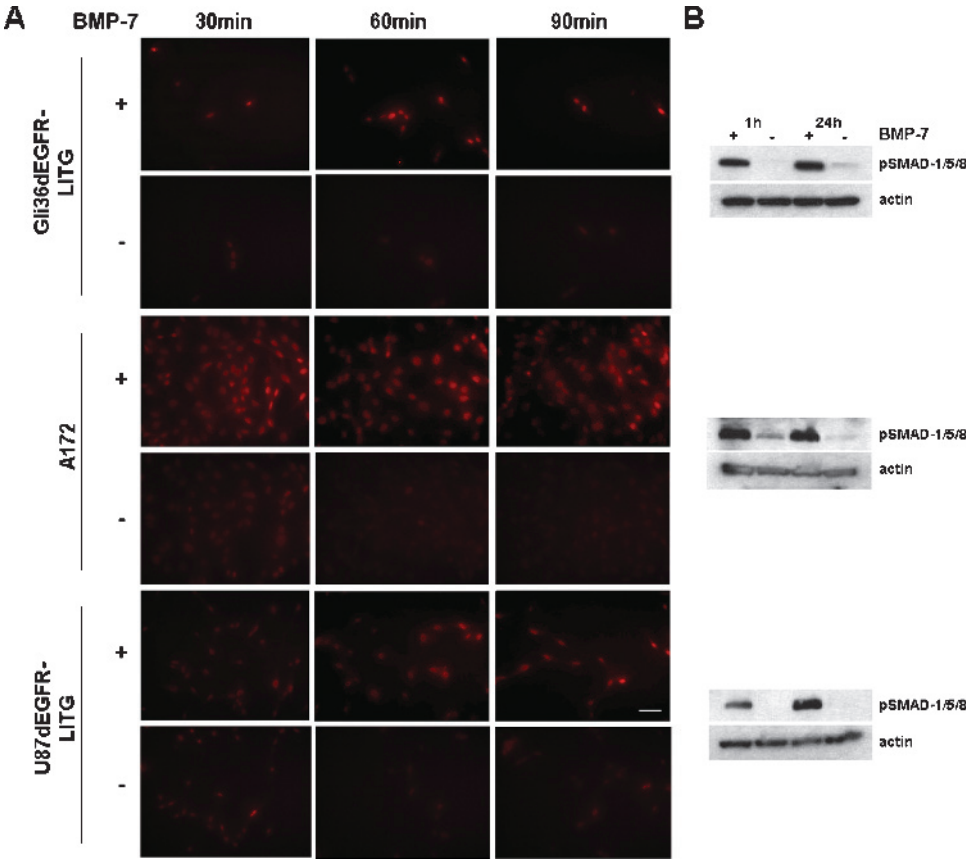

Figure 2. BMP-7 signal transduction monitored by detection of phosphorylated SMAD-1/-5/-8 (pSMAD-1/-5/-8) protein. Increasing amounts of pSMAD-1/-5/-8 were analyzed either by immunofluorescence staining of cells 30, 60, and 90 minutes after treatment with recombinant BMP-7 (500 ng/ml) (+) or control buffer (−) (*d* = ΔEGFR) (A) or by immunoblot analysis of cell lysates, obtained 1 and 24 hours after analogous cytokine treatment (B). Equally loaded protein amounts were demonstrated by detection of β-actin. Cells were photographed at 400× magnification (bar = 100 μm).

was increased, although these differences were not statistically significant (Figure 3*B*).

Because of the highest sensitivity to BMP-7 treatment, we decided to proceed to a detailed analysis of Gli36ΔEGFR-LITG cells.

BMP-7 Stimulation Decreases Gli36ΔEGFR-LITG Cell Proliferation

In the further experiments, we analyzed the influence of BMP-7 on Gli36ΔEGFR-LITG cell proliferation and apoptosis (Figure 4).

In comparison to control buffer treated cells, numbers of proliferating Gli36ΔEGFR-LITG cells decreased significantly 24 to 48 hours after BMP-7 treatment (Figure 4*A*). However, cell numbers were increased thereafter, suggesting that either BMP-7 has a basic effect on proliferation or that its stability in culture is timely limited (data not shown). To test these hypothesis, we retreated the cells after 48 hours with fresh cytokine and obtained a statistically significant growth inhibition with up to 50% decrease of cell number within 96 hours of cytokine stimulation when compared with control buffer–treated cells (Figure 4*A*), thereby also suggesting that BMP-7 has a limited life span.

In addition, we also monitored cell proliferation *in vitro* by optical imaging of luciferase activity 48 hours after BMP-7 or control buffer treatment (Figure 4*B*). The total flux value obtained by bioluminescence imaging of cytokine-treated cells was considerably lower compared with the total flux value of imaged control buffer–treated cells.

To monitor apoptotic effects, we analyzed caspase-3/-7 activity after BMP-7 and control buffer treatment (Figure 4*C*). As before, Gli36ΔEGFR-LITG cells were treated 48 hours after the initial stimulation with fresh cytokine. Caspase activity was only weakly enhanced in BMP-7–treated cells after 24 hours. However, after 48 and 96 hours of BMP-7 stimulation, the response changed. We observed increased caspase activity in control cells, whereas cytokine treatment rescued cells from serum starvation. In comparison to control buffer–treated cells, caspase activity was diminished up to 61.8% 96 hours after BMP-7 stimulation.

BMP-7 Increased the Expression of CdkIs p21 and p27 and Decreased the Phosphorylation of Cdk2 and pRb

The cell cycle analysis showed that most BMP-7–treated Gli36ΔEGFR-LITG cells were arrested in the G_1 phase of the cell cycle. To analyze how BMP-7 signaling influences the proliferation of these cells, we investigated the effects of BMP-7 on the expression of CdkIs and downstream Cdk2 and Rb phosphorylation.

BMP-7 treatment did not alter the expression of $p15^{INK4B}$ at no time point analyzed (Figure 5*A*). However, the expression of $p21^{Cip1}$ was strongly and that of $p27^{Kip1}$, to a lower extent, enhanced after BMP-7 treatment (Figure 5*A*). This is clearly demonstrated after normalization to the corresponding actin expression (Figure 5*B*). The BMP-7 effect was much stronger on $p21^{Cip1}$ expression, whose expression was increased up to 75% between 6 and 24 hours of cytokine

treatment compared with control cell lysates. During this cytokine incubation period, $p27^{Kip1}$ expression was also found to be elevated up to 40% in comparison to corresponding controls (Figure 5*A*).

Furthermore, we analyzed the phosphorylation of Cdk2 at threonine 160, which is essential for the enzymatic activity of this cell cycle–regulated kinase [30]. A striking reduction of Cdk2 phosphorylation was observed already after 1 hour of BMP-7 treatment (Figure 5*D*).

Consequently, hypophosphorylation of Rb was detected after 24 hours of cytokine treatment. We could clearly demonstrate up to 32% less phosphorylation intensities at serine 807/811 as well as at serine 795 (Figure 5*C*).

Bioluminescence Imaging of BMP-7–Triggered Antiproliferative Effects In Vivo

By *in vitro* analysis, we know that BMP-7 affects the proliferation of Gli36ΔEGFR-LITG cells. To analyze whether these findings have implications for the growth of these tumor cells *in vivo*, we performed bioluminescence imaging of luciferase activity in mice bearing experimental gliomas undergoing BMP-7 treatment (Figure 6).

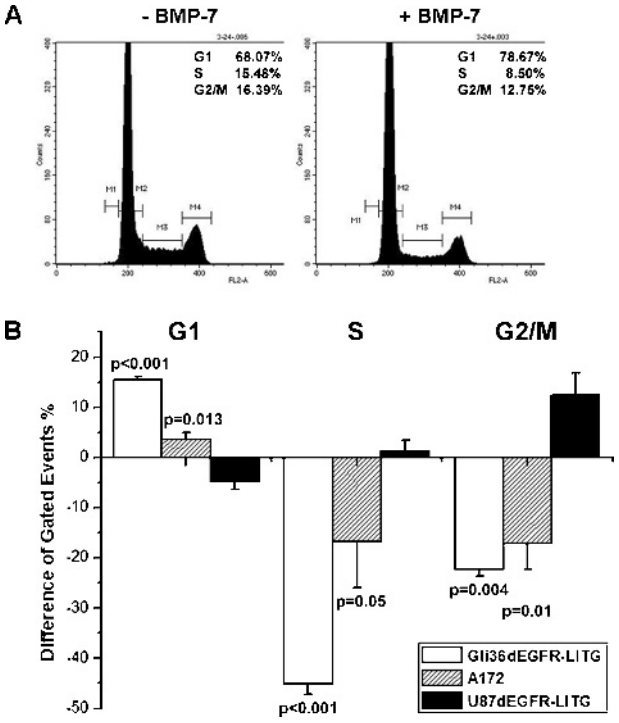

Figure 3. Cell cycle analysis of glioblastoma-derived cell lines. Cells were treated for 24 hours with recombinant BMP-7 (500 ng/ml) or control buffer and subjected to FACS analysis after propidium iodide staining of cellular DNA. The *y*-axis denotes cell count, and the *x*-axis represents DNA content. Each graph demonstrates a representative of three independent experiments. Numbers of cells being in the G_1, S, and G_2/M phases are presented in the right upper corner of each graph and display the mean values of all experiments. (A) Gli36ΔEGFR-LITG cells. (B) Cell cycle analysis of Gli36ΔEGFR-LITG, A172, and U87ΔEGFR-LITG cells. Quantification of cell numbers being in G_1, S, and G_2/M phases after BMP-7 treatment is presented in percent difference compared with numbers of control buffer–treated cells (100%). Analyzed cell lines are depicted in the legend of the graph.

For this purpose, Gli36ΔEGFR-LITG cells were implanted intracranially into nude mice, and after tumor formation, mice were treated daily with recombinant BMP-7 or control buffer. Bioluminescence imaging revealed altered growth of experimental gliomas in mice receiving BMP-7 therapy compared with untreated controls. On cytokine treatment, the increase of luciferase activity we have detected up to 10 days was dramatically lower than that detected in buffer-treated control animals. Enzyme activity in control animals reached 29-fold higher values compared with values obtained on day 0, whereas luciferase activity in BMP-7–treated animals increased only 9.5-fold after 10 days of cytokine therapy (Figure 6*A*).

The differences in tumor growth *in vivo* were observed as soon as 3 days after BMP-7 treatment, when total flux values were 6.6-fold higher in control animals compared with total flux values measured in cytokine-treated animals. At this early time point, luciferase activity was decreased up to 68% after BMP-7 stimulation in contrast to buffer-treated control mice (Figure 6, *A* and *B*). Furthermore, by immunohistochemical analysis of Ki67 and TUNEL-positive tumor cells, we could show that decreased luciferase activity resulted from diminished tumor cell proliferation and was not due to induced apoptosis (Figures W1–W3).

Discussion

In this report, we provide evidence on the potential therapeutic effectiveness of the tumor-suppressive functions of BMP-7 in human glioma–derived cells. Our experiments underline the crucial role of the BMP-7/TGF-β signaling in the regulation of glioma cell proliferation and, therefore, as possible and promising novel target in glioma therapy.

In recent years, several reports have described a tumor-suppressive function of BMP-7. The antitumorigenic effects of BMP-7 were not only directed to tumor cells but also influenced tumor-initiating cells, as it has been shown for human glioblastoma [22]. Tumor cells of epithelial origin, like colon, androgen-insensitive prostate, anaplastic thyroid, and breast carcinoma cells, respond to BMP-7 treatment with growth suppression [16,17,19,20]. The increased expression of $p21^{Cip1/Waf1}$ that we have observed on treatment of glioma cells with BMP-7 paralleled the observations made in BMP-7–treated anaplastic thyroid carcinoma cells, which displayed increased expression of $p21^{Cip1/Waf1}$ and $p27^{Kip1}$, followed by cell cycle arrest through inactivation of Cdk2 and Cdk6 [17]. Estradiol-treated MCF-7 breast cancer cells expressed augmented amounts of $p21^{Cip1/Waf1}$ after BMP-2 stimulation, which led to an inhibition of estradiol-induced cyclin D1–associated kinase and Cdk2 activity [18]. In the case of TGF-β, it has been shown that the cytokine upregulates the expression of $p15^{INK4B}$ and $p21^{Cip1/Waf1}$ and downregulates the expression of c-*myc*, resulting in the inhibition of cell proliferation [12]. However, BMP-7 did not show to have any effect on $p15^{INK4B}$ expression in Gli36ΔEGFR-LITG cells. The same was true in BMP-7–treated androgen-insensitive prostate carcinoma cells, where the cytokine did not influence the expression of $p15^{INK4B}$ and c-*myc*, but increased the expression of $p21^{Cip1/Waf1}$, which inhibited Cdk2 activity [19]. Therefore, BMP-7–mediated growth arrest might be transduced independently from $p15^{INK4B}$ and differ from TGF-β–induced signaling pathways. Nevertheless, besides $p15^{INK4B}$, also other INK4A proteins, like $p16^{INK4A}$, $p18^{INK4C}$, and $p19^{INK4D}$, could be responsible for arresting cells in G_1 because they specifically inhibit Cdk4 and Cdk6. We did not investigate $p18^{INK4C}$ or $p19^{INK4D}$, but it has been shown

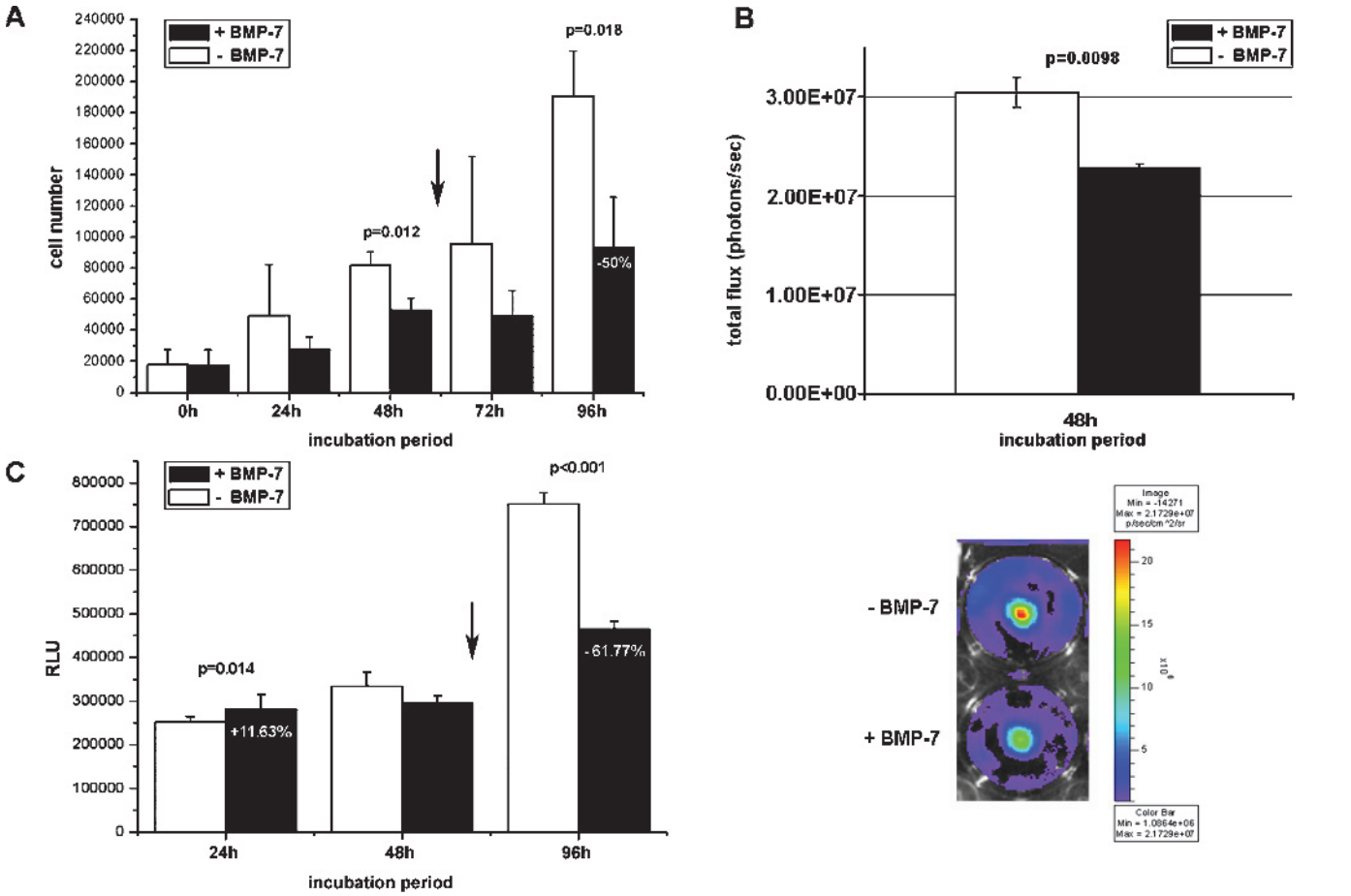

Figure 4. Analysis of cell proliferation and apoptosis in Gli36ΔEGFR-LITG cells. (A) Proliferation of cells was monitored after Trypan blue exclusion of dead cells and counting viable cells at several time points before (0 hour) and after (24, 48, 72, and 96 hours) BMP-7 (500 ng/ml) or control buffer treatment. All values are presented as the mean ± SD of six independent experiments. *P* values are depicted in the figure. (B) Cell proliferation monitored by bioluminescence imaging. Luciferase activity was imaged 48 hours after BMP-7 (500 ng/ml) or control buffer treatment, and this is presented as total flux values (photons/sec). All values are presented as the mean ± SD of three independent experiments. *P* value is depicted in the figure ($P \leq .01$). The image demonstrates a representative of three independent experiments. (C) Caspase-3/-7 activity was assessed by homogeneous luminescent caspase assay, and this is presented as relative light units (RLUs). All values are presented as the mean ± SD of three independent experiments. *P* values are depicted in the figure. Arrows indicate second treatment of cells with recombinant BMP-7 (500 ng/ml) or control buffer 48 hours after initial cytokine treatment.

that Gli36ΔEGFR-LITG cells carry a p16-CDKN2A homozygous deletion, thus we can exclude the involvement of $p16^{INK4A}$ in this context [31].

Among all cell lines tested in our study, Gli36ΔEGFR-LITG cells (and also Gli36wt cells) revealed the highest sensitivity to BMP-7 treatment resulting in growth arrest. The same was true for A172 cells, yet the effect after cytokine treatment was weaker but still significant. However, U87ΔEGFR-LITG cells responded slower to BMP-7 stimulation and showed an opposite behavior during cell cycle analysis, which was probably owing to increased apoptosis of cells rather than growth arrest. We showed that these three cell lines represent different expression profiles of BMP-7, Alk-6, Smad-6, and TGF-β_2 transcripts, which might explain their divergent responses to BMP-7 treatment. Detailed analysis on protein functionality of BMP-7, its receptors and downstream signaling molecules in these cell lines, needs to be performed to clarify these effects. We propose that the differences between the cell lines used are not due to endogenous expression of BMP-7 but are due to downstream events. Interestingly, Gli36ΔEGFR-LITG cells carry a missense mutation in both alleles of the *p53* gene, A172 cells carry only one mutated allele, and U87ΔEGFR-LITG cells are p53 wild type [32–34]. Analyzing the differences of expression and functionality of downstream signaling events will be of great importance also regarding the clinical relevance of glioblastoma therapy.

The antiproliferative effects of BMP-7 on Gli36ΔEGFR-LITG cells presented in this study were detected when cells were cultured under serum starvation (1% serum), whereas no efficient inhibition of proliferation was achieved in the presence of regular growth medium (10% serum; data not shown). In agreement with our findings, it has been shown that, in the presence of 10% serum, BMP-7 does not induce phosphorylation of Smad-1/-5 or expression of Id-1 in PC-3 cells [19]. The authors suggested that FCS might either contain antagonists of BMP signals, such as Noggin and chordin, or induce their expression. Besides antagonists of BMP signaling, also counteracting cytokines, possibly present in the serum (not heat-inactivated), might affect cell proliferation. However, the specific inhibition of TGF-β/activin signaling through Alk-4, -5, and -7 in the presence of 10% serum did not induce growth suppression by BMP-7 in PC-3 cells [19].

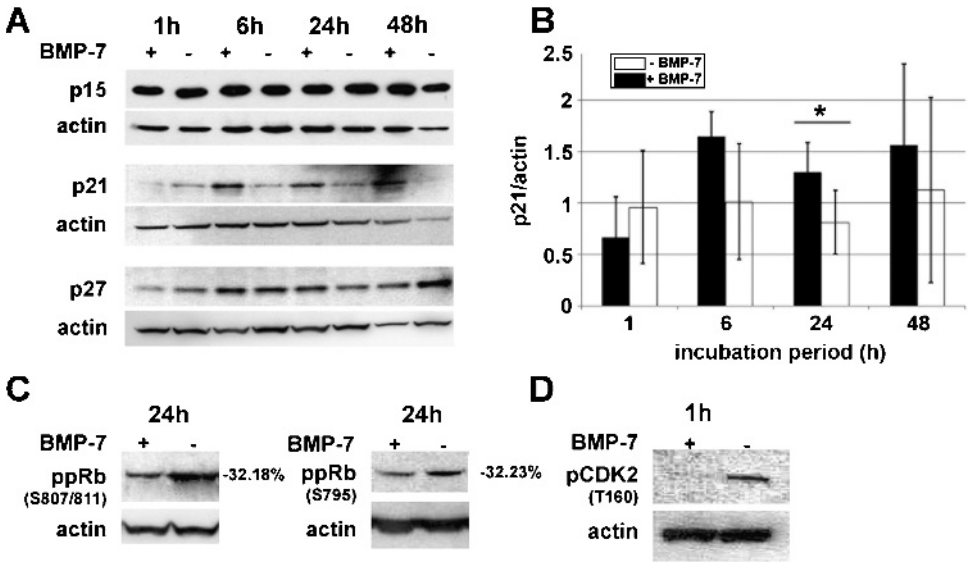

Figure 5. Immunoblot analysis of Cdk inhibitors. Gli36ΔEGFR-LITG cell lysates were obtained after several time points of BMP-7 (500 ng/ml) or control buffer treatment. (A) Protein expression of p15, p21, and p27. (B) Densitometric quantification of p21 protein expression after normalization to β-actin protein expression. Differences of p21 protein amounts are presented as arbitrary units and resulted from quantification of three independent experiments (*$P \leq .05$). (C) Hypophosphorylation of Rb (Ser807/811, Ser795) could be detected 24 hours after cytokine treatment. Quantification of Rb phosphorylation intensities of BMP-7–treated cells is presented as percent difference compared with Rb phosphorylation intensities of control buffer–treated cells (100%) and resulted from quantification of two independent experiments. (D) Decreased phosphorylation of Cdk2 (Thr160) was observed 1 hour after addition of BMP-7. Detection of β-actin protein served as a loading control of each experiment, and this is presented for all corresponding Western blots.

The activity of caspase-3/-7 was clearly enhanced in buffer-treated control cells compared with BMP-7–treated ones, suggesting that the cytokine rescued Gli36ΔEGFR-LITG cells from serum starvation. BMPs (BMP-7 and -2) have been shown to protect cells from stress-induced apoptosis. In C4-2B cells but not in LNCaP cells, a serum starvation–induced decrease of survivin was counteracted by BMP-7, whereas expression levels of Bcl-xl, Bax, and XIAP remained unaffected, pointing out antiapoptotic effects of BMPs [35].

However, taking into account that the proliferation of Gli36ΔEGFR-LITG cells was impaired and cell cycle analysis displayed an arrest of cells in the G_1 phase, we conclude that BMP-7 induced cell cycle arrest in the late G_1 phase by upregulation of CdkI $p21^{Cip1/Waf1}$, which inhibited Cdk2 activation directly or by inhibiting Cdk4/Cdk6 in the mid and late G_1 phase.

Because *in vitro* analysis not always reflects exactly the *in vivo* situation, mouse experiments approaching *in vivo* conditions are essentially

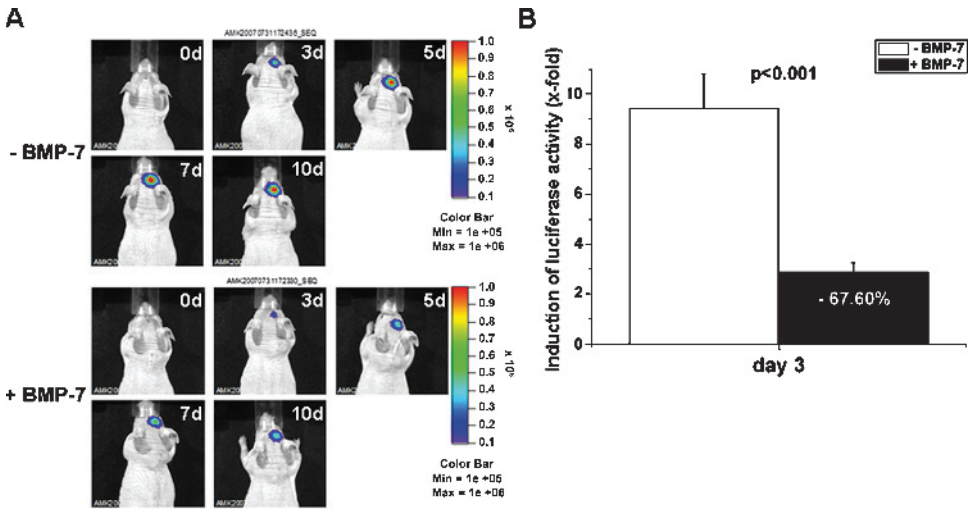

Figure 6. *In vivo* bioluminescence imaging of luciferase activity in experimental gliomas. (A) Optical imaging of luciferase activity in BMP-7–treated (lower panel) and buffer-treated (upper panel) nude mice 0, 3, 5, 7, and 10 days after the start of BMP-7/buffer treatment. (B) Quantification of luciferase activity 3 days after the start of BMP-7 therapy ($n = 6$) compared with buffer-treated control mice ($n = 6$). Luciferase activity at day 3 is presented as *x*-fold induction of total flux (photons/sec) normalized to total flux values at day 0 for BMP-7– and buffer-treated mice, respectively.

needed to prove cell culture results. Bioluminescence imaging represents a useful and highly sensitive technique to study glioma cell proliferation and effects of antiproliferative compounds [36,37]. Shah et al. [38] monitored both gene delivery and efficacy of TRAIL-induced apoptosis in experimental brain tumors *in vivo* by dual-enzyme substrate bioluminescence imaging. After intracranial implantation of Gli36ΔEGFR-LITG cells, we were able to monitor the dynamics of the antiproliferative effects of BMP-7 by optical imaging *in vivo* and confirmed our experiments in cell culture. In fact, BMP-7 treatment impaired the growth of experimental gliomas, clearly demonstrated by bioluminescence imaging of luciferase activity that was diminished up to 68% in BMP-7–treated animals compared with buffer-treated control mice 3 days after starting the treatment (Figure W4). More importantly, this antiproliferative effect of BMP-7 caused a blockage of tumor growth up to 10 days, thus suggesting a potential use of BMP-7 for glioma treatment. *In vivo* bioluminescence imaging of luciferase activity together with magnetic resonance imaging and positron emission tomography has been confirmed to be a powerful and quantitative tool for the assessment of antineoplastic therapies in living animals [39–41]. These and other authors suggested that imaging luciferase activity represents advantages over direct tumor volume measurements because it provides a quantitative surrogate measure of the metabolically active tumor cells excluding necrotic cells unable to emit photons [38,39].

The divergent responses to BMP-7 of different cell lines that we found *in vitro* seem to originate from varying downstream signaling molecules and might also reflect the diversity of primary gliomas. Screening the expression profiles and functionality of BMP-7/TGF-β signaling molecules in primary gliomas could help to distinguish between responders and potential nonresponders. Regarding primary gliomas, BMPs also inhibit the proliferation of cancer stem cells by inducing differentiation of these cells [22]. More recently, opposite effects of BMPs on cancer stem cells have been reported when the expression pattern of BMPR is disturbed[23]. Supporting our findings in glioma cell lines, the expression of downstream signaling molecules in cancer stem cells also seem to determine BMP responsiveness, pointing out the necessity of detailed screening studies in patients with gliomas.

In conclusion, we demonstrate that BMP-7 induces cell cycle arrest at the G_1/S checkpoint and, therefore, reduces the proliferation of human glioma–derived Gli36ΔEGFR-LITG cells. BMP-7 treatment increased the expression of CdkI $p21^{Cip1}$, which led to a decreased level of activated Cdk2 and hypophosphorylation of pRb. Taken together with our *in vivo* analysis, we were able to noninvasively image and quantify these antiproliferative effects of BMP-7 *in vivo*. These results underline the potential role of targeting the BMP/TGF-β signaling cascade for generating novel molecular approaches in cancer and especially glioblastoma therapy.

Acknowledgments

The authors thank P. Zigrino for carefully reading the article and G. Schneider and A. Wilbrand-Hennes for excellent technical assistance.

References

[1] Blumenthal DT and Schulman SF (2005). Survival outcomes in glioblastoma multiforme, including the impact of adjuvant chemotherapy. *Expert Rev Neurother* **5**, 683–690.

[2] Gold LI (1999). The role for transforming growth factor-β (TGF-β) in human cancer. *Crit Rev Oncog* **10**, 303–360.

[3] Elliott RL and Blobe GC (2005). Role of transforming growth factor β in human cancer. *J Clin Oncol* **23**, 2078–2093.

[4] Golestaneh N and Mishra B (2005). TGF-β, neuronal stem cells and glioblastoma. *Oncogene* **24**, 5722–5730.

[5] Derynck R and Zhang YE (2003). Smad-dependent and Smad-independent pathways in TGF-β family signalling. *Nature* **425**, 577–584.

[6] Akhurst RJ and Derynck R (2001). TGF-β signaling in cancer—a double-edged sword. *Trends Cell Biol* **11**, S44–S51.

[7] Massague J (1998). TGF-β signal transduction. *Annu Rev Biochem* **67**, 753–791.

[8] Ducy P and Karsenty G (2000). The family of bone morphogenetic proteins. *Kidney Int* **57**, 2207–2214.

[9] Feng XH and Derynck R (2005). Specificity and versatility in TGF-β signaling through Smads. *Annu Rev Cell Dev Biol* **21**, 659–693.

[10] Miyazono K, Maeda S, and Imamura T (2005). BMP receptor signaling: transcriptional targets, regulation of signals, and signaling cross-talk. *Cytokine Growth Factor Rev* **16**, 251–263.

[11] Lee KY and Bae SC (2002). TGF-β–dependent cell growth arrest and apoptosis. *J Biochem Mol Biol* **35**, 47–53.

[12] Massague J, Blain SW, and Lo RS (2000). TGFβ signaling in growth control, cancer, and heritable disorders. *Cell* **103**, 295–309.

[13] Weinberg RA (1995). The retinoblastoma protein and cell cycle control. *Cell* **81**, 323–330.

[14] Wach S, Schirmacher P, Protschka M, and Blessing M (2001). Overexpression of bone morphogenetic protein-6 (BMP-6) in murine epidermis suppresses skin tumor formation by induction of apoptosis and downregulation of *fos/jun* family members. *Oncogene* **20**, 7761–7769.

[15] Ro TB, Holt RU, Brenne AT, Hjorth-Hansen H, Waage A, Hjertner O, Sundan A, and Borset M (2004). Bone morphogenetic protein-5, -6 and -7 inhibit growth and induce apoptosis in human myeloma cells. *Oncogene* **23**, 3024–3032.

[16] Beck SE, Jung BH, Fiorino A, Gomez J, Rosario ED, Cabrera BL, Huang SC, Chow JY, and Carethers JM (2006). Bone morphogenetic protein signaling and growth suppression in colon cancer. *Am J Physiol Gastrointest Liver Physiol* **291**, G135–G145.

[17] Franzen A and Heldin NE (2001). BMP-7–induced cell cycle arrest of anaplastic thyroid carcinoma cells via p21(CIP1) and p27(KIP1). *Biochem Biophys Res Commun* **285**, 773–781.

[18] Ghosh-Choudhury N, Ghosh-Choudhury G, Celeste A, Ghosh PM, Moyer M, Abboud SL, and Kreisberg J (2000). Bone morphogenetic protein-2 induces cyclin kinase inhibitor p21 and hypophosphorylation of retinoblastoma protein in estradiol-treated MCF-7 human breast cancer cells. *Biochim Biophys Acta* **1497**, 186–196.

[19] Miyazaki H, Watabe T, Kitamura T, and Miyazono K (2004). BMP signals inhibit proliferation and *in vivo* tumor growth of androgen-insensitive prostate carcinoma cells. *Oncogene* **23**, 9326–9335.

[20] Buijs JT, Henriquez NV, van Overveld PGM, van der Horst G, Que I, Schwaninger R, Rentsch C, ten Dijke P, Cleton-Jansen A-M, Notting IC, et al. (2007). Bone morphogenetic protein 7 in the development and treatment of bone metastases from breast cancer. *Cancer Research* **67**, 8742–8751.

[21] Yamada N, Kato M, ten Dijke P, Yamashita H, Sampath TK, Heldin CH, Miyazono K, and Funa K (1996). Bone morphogenetic protein type IB receptor is progressively expressed in malignant glioma tumours. *Br J Cancer* **73**, 624–629.

[22] Piccirillo SG, Reynolds BA, Zanetti N, Lamorte G, Binda E, Broggi G, Brem H, Olivi A, Dimeco F, and Vescovi AL (2006). Bone morphogenetic proteins inhibit the tumorigenic potential of human brain tumour-initiating cells. *Nature* **444**, 761–765.

[23] Lee J, Son MJ, Woolard K, Donin NM, Li A, Cheng CH, Kotliarova S, Kotliarov Y, Walling J, Ahn S, et al. (2008). Epigenetic-mediated dysfunction of the bone morphogenetic protein pathway inhibits differentiation of glioblastoma-initiating cells. *Cancer Cell* **13**, 69–80.

[24] Jacobs AH, Winkeler A, Hartung M, Slack M, Dittmar C, Kummer C, Knoess C, Galldiks N, Vollmar S, Wienhard K, et al. (2003). Improved herpes simplex virus type 1 amplicon vectors for proportional coexpression of positron emission tomography marker and therapeutic genes. *Hum Gene Ther* **14**, 277–297.

[25] Vindelov LL, Christensen IJ, Jensen G, and Nissen NI (1983). Limits of detection of nuclear DNA abnormalities by flow cytometric DNA analysis. Results obtained by a set of methods for sample-storage, staining and internal standardization. *Cytometry* **3**, 332–339.

[26] Vindelov LL, Christensen IJ, Keiding N, Spang-Thomsen M, and Nissen NI (1983). Long-term storage of samples for flow cytometric DNA analysis. *Cytometry* **3**, 317–322.

[27] Vindelov LL, Christensen IJ, and Nissen NI (1983). Standardization of high-resolution flow cytometric DNA analysis by the simultaneous use of chicken and trout red blood cells as internal reference standards. *Cytometry* **3**, 328–331.

[28] Vindelov LL, Christensen IJ, and Nissen NI (1983). A detergent-trypsin method for the preparation of nuclei for flow cytometric DNA analysis. *Cytometry* **3**, 323–327.

[29] Klose A, Wilbrand-Hennes A, Zigrino P, Weber E, Krieg T, Mauch C, and Hunzelmann N (2006). Contact of high-invasive, but not low-invasive, melanoma cells to native collagen I induces the release of mature cathepsin B. *Int J Cancer* **118**, 2735–2743.

[30] Desai D, Gu Y, and Morgan DO (1992). Activation of human cyclin–dependent kinases *in vitro*. *Mol Biol Cell* **3**, 571–582.

[31] Saydam O, Glauser DL, Heid I, Turkeri G, Hilbe M, Jacobs AH, Ackermann M, and Fraefel C (2005). Herpes simplex virus 1 amplicon vector–mediated siRNA targeting epidermal growth factor receptor inhibits growth of human glioma cells *in vivo*. *Mol Ther* **12**, 803–812.

[32] Abe T, Wakimoto H, Bookstein R, Maneval DC, Chiocca EA, and Basilion JP (2002). Intra-arterial delivery of p53-containing adenoviral vector into experimental brain tumors. *Cancer Gene Ther* **9**, 228–235.

[33] Li H, Lochmuller H, Yong VW, Karpati G, and Nalbantoglu J (1997). Adenovirus-mediated wild-type p53 gene transfer and overexpression induces apoptosis of human glioma cells independent of endogenous p53 status. *J Neuropathol Exp Neurol* **56**, 872–878.

[34] Prasad G, Wang H, Agrawal S, and Zhang R (2002). Antisense anti-MDM2 oligonucleotides as a novel approach to the treatment of glioblastoma multiforme. *Anticancer Res* **22**, 107–116.

[35] Yang S, Zhong C, Frenkel B, Reddi AH, and Roy-Burman P (2005). Diverse biological effect and Smad signaling of bone morphogenetic protein 7 in prostate tumor cells. *Cancer Res* **65**, 5769–5777.

[36] Winkeler A, Sena-Esteves M, Paulis LE, Li H, Waerzeggers Y, Ruckriem B, Himmelreich U, Klein M, Monfared P, Rueger MA, et al. (2007). Switching on the lights for gene therapy. *PLoS One* **2**, e528.

[37] Uhrbom L, Nerio E, and Holland EC (2004). Dissecting tumor maintenance requirements using bioluminescence imaging of cell proliferation in a mouse glioma model. *Nat Med* **10**, 1257–1260.

[38] Shah K, Tang Y, Breakefield X, and Weissleder R (2003). Real-time imaging of TRAIL-induced apoptosis of glioma tumors *in vivo*. *Oncogene* **22**, 6865–6872.

[39] Rehemtulla A, Stegman LD, Cardozo SJ, Gupta S, Hall DE, Contag CH, and Ross BD (2000). Rapid and quantitative assessment of cancer treatment response using *in vivo* bioluminescence imaging. *Neoplasia* **2**, 491–495.

[40] Jacobs AH, Rueger MA, Winkeler A, Li H, Vollmar S, Waerzeggers Y, Rueckriem B, Kummer C, Dittmar C, Klein M, et al. (2007). Imaging-guided gene therapy of experimental gliomas. *Cancer Res* **67**, 1706–1715.

[41] Kummer C, Winkeler A, Dittmar C, Bauer B, Rueger MA, Rueckriem B, Heneka MT, Vollmar S, Wienhard K, Fraefel C, et al. (2007). Multitracer positron emission tomographic imaging of exogenous gene expression mediated by a universal herpes simplex virus 1 amplicon vector. *Mol Imaging* **6**, 181–192.

Supplementary Materials and Methods

Immunohistochemistry

For the detection of proliferating and apoptotic cells in Gli36ΔEGFR-LITG cells derived experimental gliomas, mouse brains of BMP-7–treated and control animals were dissected after bioluminescence analysis of accordant tumors. Before tumor dissection, mice were perfused with 4% paraformaldehyde. Afterward, brains were postfixed for 24 hours before paraffin embedding. Immunohistochemistry was carried out using standard procedures on 4-μm sections. For the detection of proliferating tumor cells, we used the Ki67 SP6 rabbit monoclonal primary antibody (dilution 1:500, KI681C01; DCS Innovative Diagnostik-Systeme GmbH & Co KG, Hamburg, Germany) and rabbit anti–mouse biotin secondary antibody (dilution 1:200, E0413; DAKO GmbH, Hamburg, Germany) plus biotin-avidin complex (Vectastain Elite ABC Kit; Vector Laboratories, Ltd, Orton Southgate, Peterborough, UK) to detect the primary antibody. DAB (3,3′-diaminobenzidine) substrate was used to stain peroxidase activity (Vector Laboratories, Ltd).

For the detection of apoptotic cells, we used the DeadEnd Colorimetric TUNEL System according to the manufactures' instructions (Promega GmbH). Positive controls for the detection of DNA fragmentation were performed using DNase I treatment and included in each experiment. Counterstaining of cell nuclei was performed with Mayer Hämalaun solution.

Analysis of Ki67 and TUNEL-positive cells was carried out as follows: We analyzed tumor sections of two sets of animals (n = 3). One set was treated with BMP-7, and the other set was treated with control buffer. Sections that were subjected to the analysis of proliferating and apoptotic cells were derived from four different parts of each corresponding tumor (three tumors of each set of animals). After staining, sections were photographed at 200× magnification (bars = 50 μm), and Ki67 or TUNEL-positive cells were counted per visual field (three tumors of each set of animals ⇒ four sections per tumor ⇒ 1 visual field per section ⇒ 12 visual fields per set of animals). Statistical analysis was performed using Student's t test with Microsoft Office Excel. Statistical 4 tests were heteroskedastic and 2-tailed.

Table W1. Primer Pairs of TGF-β Superfamily Signaling Molecules.

	Sequence	Annealing Temperature (°C)	Extension Time	Cycles	Amplicon Size (bp)	Reference
BMP-7	For 3′ CACGCTACCACCATCGAGAG 5′ Rev 3′ TTCATGTAGGAGTTCAGAGGGA 5′	58	41 sec	35	669	PerlPrimer v1.1.10 Software
Alk-2	For 3′ CTCCGAGTACCCCAGTGA 5′ Rev 3′ CTGTGTTCCAGGGAAGGA 5′	55	30 sec	35	457	PerlPrimer v1.1.10 Software
Alk-3	For 3′ CAGAATCTGGATAGTATGCTTCATGGC 5′ Rev 3′ GACAGCCATAGAAATGAGCAAAACCAGC 5′	60	30 sec	35	418	PerlPrimer v1.1.10 Software
Alk-6	For 3′ TGCGAAGTGCAGGAAAAT 5′ Rev 3′ GGGATTCTCCAGGAGGAA 5′	55	30 sec	35	502	PerlPrimer v1.1.10 Software
BMPRII	For 3′ CATTGGAGATCCCCAAGA 5′ Rev 3′ ATATCGACCTCGGCCAAT 5′	50	30 sec	35	382	PerlPrimer v1.1.10 Software
ActrIIA	For 3′ CTTCAAATCCAGTTACACCT 5′ Rev 3′ CAGTTCATTCCAAGAGACCA 5′	53	30 sec	35	490	PerlPrimer v1.1.10 Software
ActrIIB	For 3′ GATGACTTCAACTGCTACGA 5′ Rev 3′ ATGTGATGATGTTCCCCTTGAG 5′	55	37 sec	35	612	PerlPrimer v1.1.10 Software
SMAD-1	For 3′ CATCAATCCCTACCACTATAAGAG 5′ Rev 3′ GAAACCATCCACCAACACAC 5′	56	40 sec	35	534	PerlPrimer v1.1.10 Software
SMAD-5	For 3′ TCAACCCATACCACTATAAGAG 5′ Rev 3′ CTCATATACTGCCTCAAACCC 5′	55	1 min	35	847	PerlPrimer v1.1.10 Software
SMAD-8	For 3′ CTCCCTCTTCTCCTTCACCA 5′ Rev 3′ CACCCTTTCCTATATGTCTCCT 5′	57	1 min	35	871	PerlPrimer v1.1.10 Software
SMAD-4	For 3′ TCAATTCAAACCATCCAGCA 5′ Rev 3′ GACCCAAACATCACCTTCAC 5′	56	40 sec	35	665	PerlPrimer v1.1.10 Software
TGF-β1	For 3′ TGGCGATACCTCAGCAACC 5′ Rev 3′ CTCGTGGATCCACTTCCAG 5′	59	25 sec	35	405	*Int J Cancer* 2000;89:251–258
TGF-β2	For 3′ ATCCCGCCCACTTTCTACAGAC 5′ Rev 3′ CATCCAAAGCACGCTTCTTCC 5′	61	35 sec	35	565	*Int J Cancer* 2000;89:251–258
TGF-β3	For 3′ TACTATGCCAACTTCTGCTC 5′ Rev 3′ AACTTACCATCCCTTTCCTC 5′	55	32 sec	35	522	*Int J Cancer* 2000;89:251–258
Alk-5	For 3′ ACGGCGTTACAGTGTTTCTG 5′ Rev 3′ GGTTGTGGCAGATATAGACC 5′	57	22 sec	35	358	*Int J Cancer* 2000;89:251–258
Alk-1	For 3′ CTCAGACACGACAACATCCT 5′ Rev 3′ TATAGTCCTCCACGATGCCA 5′	57	31 sec	35	513	PerlPrimer v1.1.10 Software
Tβ-RII	For 3′ AGCAACTGCAGCATCACCTC 5′ Rev 3′ TGATGTCTGAGAAGATGTCC 5′	58	42 sec	35	688	*Int J Cancer* 2000;89:251–258
SMAD-2	For 3′ ATCCTAACAGAACTTCCGCC 5′ Rev 3′ CTCAGCAAAAACTTCCCCAC 5′	57	31 sec	35	489	*Int J Cancer* 2000;89:251–258
SMAD-3	For 3′ AGAAGACGGGGCAGCTGGAC 5′ Rev 3′ GACATCGGATTCGGGGATAG 5′	57	31 sec	35	511	*Int J Cancer* 2000;89:251–258
SMAD-6	For 3′ TGAATTCTCAGACGCCAGCA 5′ Rev 3′ GCTCGAAGTCGAACACCTT 5′	55	30 sec	40	386	*Biochem Biophys Res Commun* 2001;287(1):47–55
SMAD-7	For 3′ GCCCTCTCTGGATATCTTCT 5′ Rev 3′ GCTGCATAAACTCGTGGTCA 5′	55	30 sec	35	320	*Biochem Biophys Res Commun* 2001;287(1):47–55
β-actin	For 3′ ATCTGGCACCACACCTTCTACAATGAGCTGCG 5′ Rev 3′ CGTCATACTCCTGCTTGCTGATCCACATCTGC 5′	67	1 min	25	838	PerlPrimer v1.1.10 Software

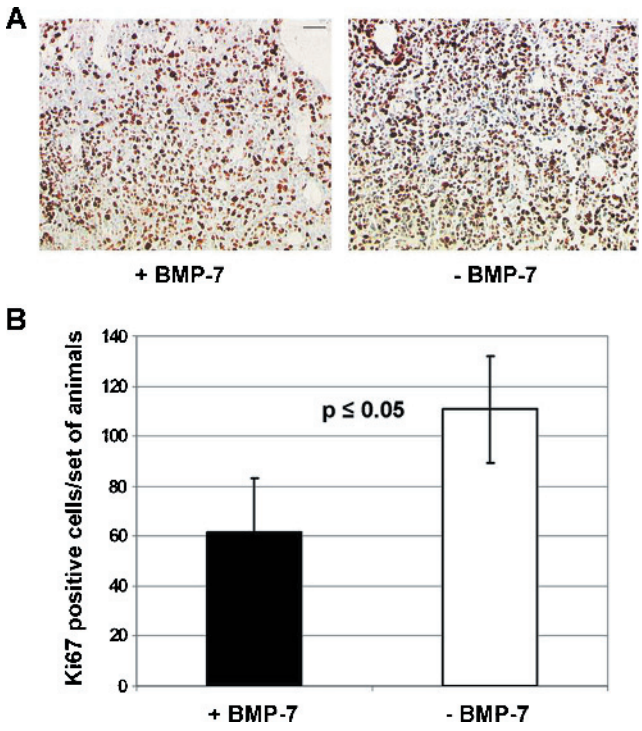

Figure W1. Immunohistochemical analysis of Ki67 in experimental gliomas. Mice brains were dissected 10 days after starting BMP-7 (100 μg/kg per day) or control buffer treatment ($\pm$ BMP-7). Sections (4 μm) of paraffin-embedded tissue were subjected to immunohistochemical analysis of Ki67 expression. (A) Representative images of mice brain sections are presented at 200$\times$ magnification (bars = 50 μm). (B) Ki67-positive cells were counted per visual field (VF); means were calculated and plotted per set of animal ($n = 3$, $P \leq .05$).

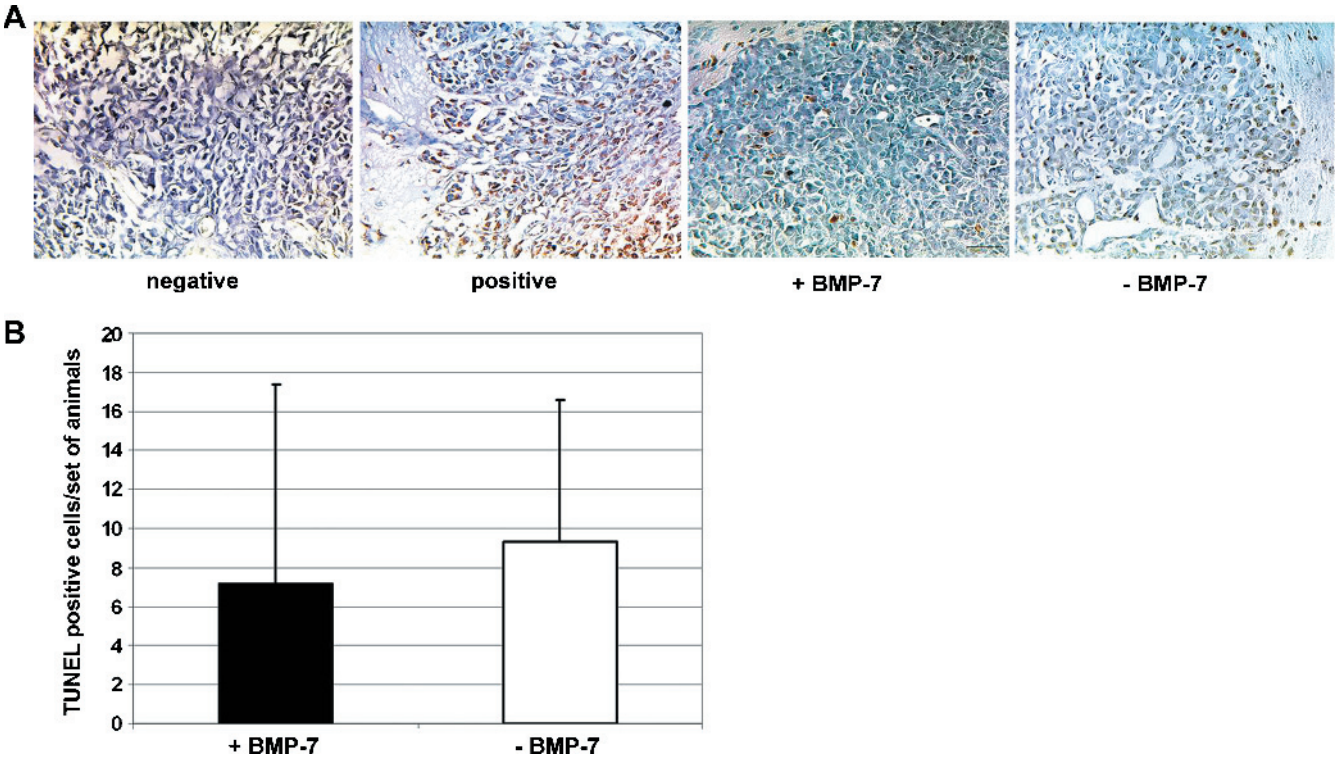

Figure W2. TUNEL analysis in experimental gliomas. Mice brains were dissected 10 days after starting BMP-7 (100 μg/kg per day) or control buffer treatment ($\pm$ BMP-7). Sections (4 μm) of paraffin-embedded tissue were subjected to immunohistochemical analysis of TUNEL-positive cells. (A) Representative images of mice brain sections are presented at 200$\times$ magnification (bars = 50 μm). Negative and positive control sections (DNase I–treated) are included. (B) TUNEL-positive cells were counted per visual field (VF); means were calculated and plotted per set of animals ($n = 3$, $P = .78$).

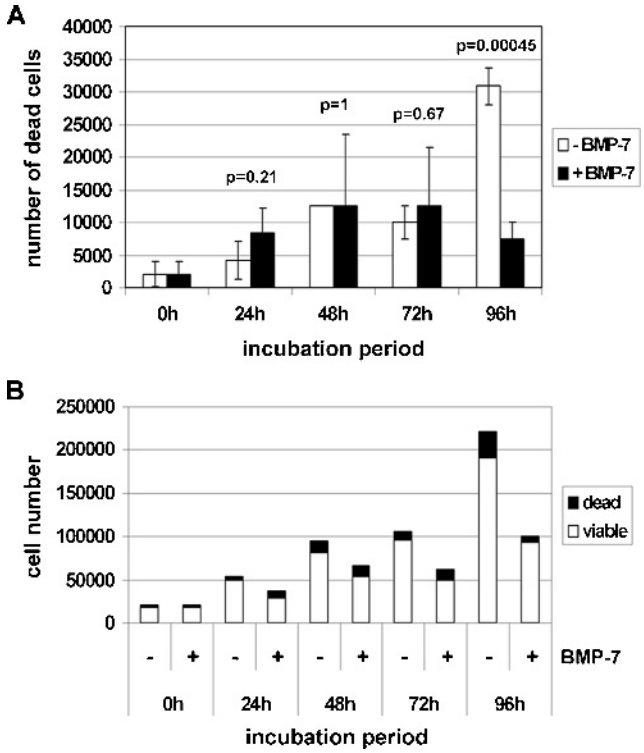

Figure W3. Numbers of viable and dead cells in the presence or absence of BMP-7. Viable and dead cells were monitored after Trypan blue exclusion and counted at several time points before (0 hour) and after (24, 48, 72, and 96 hours) BMP-7 (500 ng/ml) or control buffer treatment. All values are presented as the mean ± SD of three independent experiments. *P* values are depicted in the figure. (A) Numbers of dead cells in the absence or presence of BMP-7. (B) Fractions of viable and dead cells in the presence or absence of BMP-7.

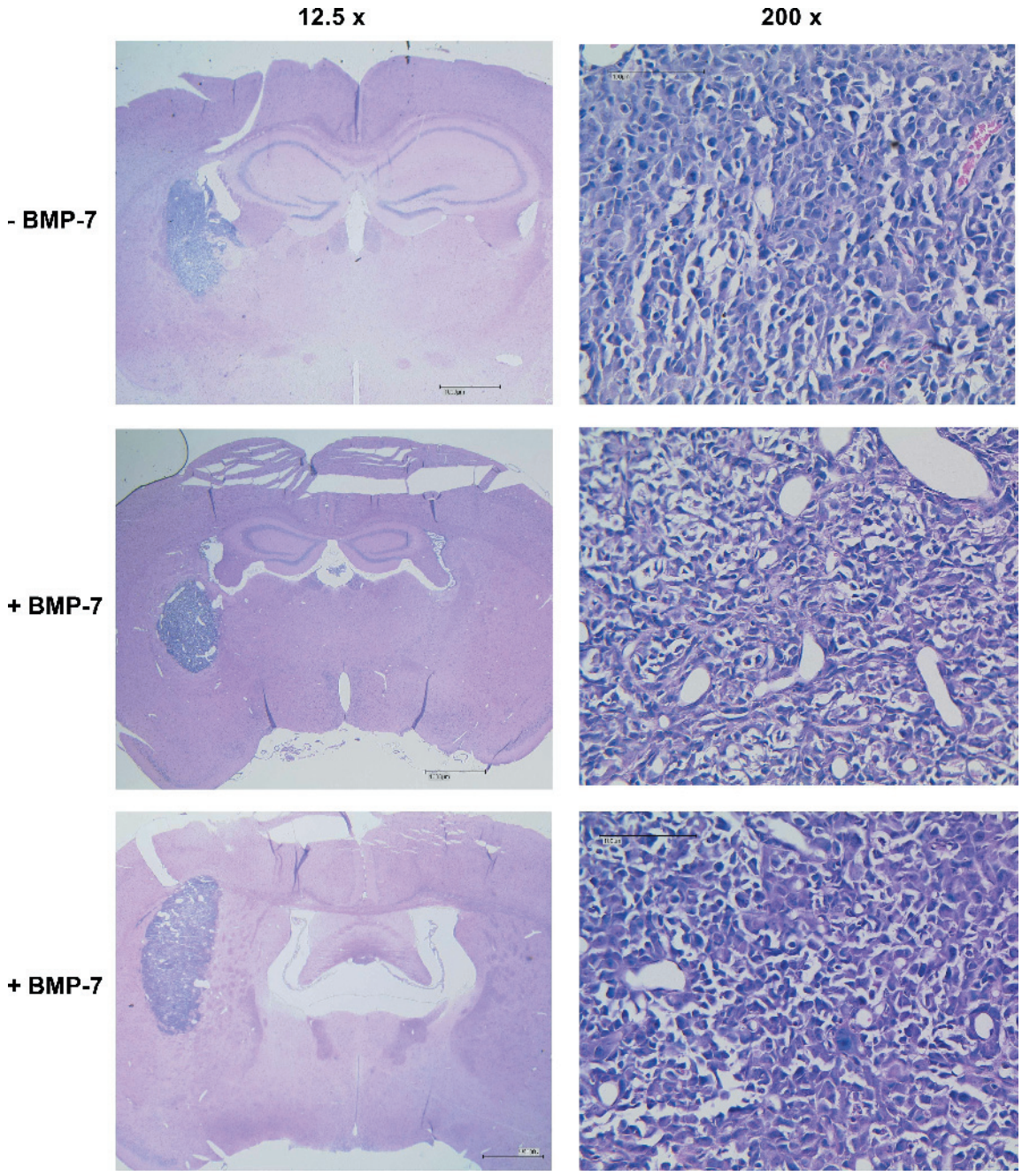

Figure W4. Hematoxylin and eosin staining of experimental gliomas. Mice brains were dissected 10 days after starting BMP-7 (100 μg/kg per day) or control buffer treatment ($\pm$ BMP-7). Sections (4 μm) of paraffin-embedded tissue were subjected to hematoxylin and eosin staining. Representative images of mice brain sections are presented at 12.5$\times$ and 200$\times$ magnifications (bars = 1000 μm and 100 μm, respectively).